IEEE Access
Multidisciplinary | Rapid Review | Open Access Journal

Received September 26, 2020, accepted October 6, 2020, date of publication October 20, 2020, date of current version November 2, 2020.

Digital Object Identifier 10.1109/ACCESS.2020.3032384

A Stiffness Adjustable 6-DOF Robotic System for Pituitary Tumor Resection Under MRI

MUHAMMAD UMAR FAROOQ[1], (Graduate Student Member, IEEE), HYUNWOO BAEK[2], SUNGMIN SEUNG[3], KYOUNGRAE CHA[3,4], HEON YOU[5], DONG-SOO KWON[2,6], (Senior Member, IEEE), AND SEONG YOUNG KO[1], (Member, IEEE)

[1]Department of Mechanical Engineering, Chonnam National University, Gwangju 61186, South Korea
[2]Department of Mechanical Engineering, Korea Advanced Institute of Science and Technology, Daejeon 34141, South Korea
[3]Daegu-Gyeongbuk Medical Innovation Foundation, Daegu 41061, South Korea
[4]Korea Institute of Medical Microrobotics, Gwangju 61011, South Korea
[5]National Cancer Center, Goyang 10408, South Korea
[6]EasyEndo Surgical Inc., Daejeon 34051, South Korea

Corresponding author: Seong Young Ko (sko@jnu.ac.kr)

This work was supported in part by the Ministry of Trade, Industry and Energy (MOTIE), South Korea, through the Industrial Technology Innovation Program, under Grant 10080609, and in part by the Ministry of Health and Welfare, South Korea, through the Korea Health Technology Development Research and Development Project through the Korea Health Industry Development Institute (KHIDI), under Grant HI19C0642.

ABSTRACT Magnetic resonance imaging offers better visualization for tumors present in the delicate parts of the human body. A pituitary tumor is one of the common types of brain-related tumors located underside the brain. It can be accessed through the nostrils and visualized better using magnetic resonance imaging (MRI). In this work, we present a 6-degree-of-freedom (DOF) robotic system for pituitary tumor resection via a transsphenoidal approach designed specifically for a commercially available 3T MRI scanner. The robotic system is designed to follow the anatomical and surgical constraints and to work inside the bore of the MRI to allow image acquisition during the surgical procedure. It has a 6-DOF manipulator consisting of a concentric tube and a tendon-driven bendable section. Both mechanisms are merged to have stiffness changing capability, and payload capacity to aid the surgical task. The manipulator is attached to a flexure shaft to bend it at the desired surgical angles. The materials used for development are analyzed in MRI and exhibit signal-noise ratio (SNR) reduction of less than 10%. The experimental results show that the stiffness can be changed more than ten times for safe navigation to the surgical site without damaging the surrounding tissues. Also, it can provide a maximum lifting force of more than 2N. The presented system is the preliminary version of the pituitary tumor resection system under development and shows the feasibility to be used in a real surgical environment.

INDEX TERMS Concentric tube robot (CTR), magnetic resonance imaging (MRI), neurosurgery, pituitary tumor resection, stiffness changing capability.

I. INTRODUCTION

Neurosurgery is one of the complex procedures requiring accurate, precise, and dexterous tools to efficiently carry out the task. The pituitary gland also called the master gland, controls the secretion of other glands. It is located between the hypothalamus and the pineal gland and can be accessed through the nose. Pituitary tumor accounts for 10% of the overall brain-related tumors and normally appears in the third or fourth decade of life [1]. Due to the ease of access, usually, a trans-sphenoidal route is used to remove the tumor. An endoscope is inserted in the nasal cavity through the nostril to reach the pituitary gland [2] but it is difficult to distinguish between the normal tissue and tumor using the endoscopic view. Magnetic resonance imaging (MRI) provides better vision when compared to other imaging techniques [3]. For pituitary tumors, MRI is the most suited technique as it provides a clearer location and extension of the tumor and the surrounding tissues [1].

Robotics has provided many solutions for different surgical procedures including the brain, heart, and nose, etc. [4]. The first robotic system for neurosurgery (Unimation Puma

The associate editor coordinating the review of this manuscript and approving it for publication was Hamid Mohammad-Sedighi.

200) was deployed three decades ago [5]. After that, many tools and systems have been developed for neurosurgery and MR guided interventions. A biopsy needle system for prostate interventions in MRI was developed in [6]–[8] while [9], [10] presents the breast biopsy system for MRI. NeuroArm is a robotic system developed for specially designed intra-operative MRI and can be deployed for different surgical procedures including brain surgery [11]. A Neuroendoscopic surgical system has also been developed previously for open type brain surgery (also called a craniotomy) under MRI [12]. RAVEN is another semi-autonomous brain tumor ablation robot with visual feedback but lacks compatibility in MRI [13]. An MR guided robotically actuated stereotactic neurosurgical system is presented in [14] that improves the accuracy and efficiency of the procedure. All the above brain surgery robots are feasible for open type procedures and their usage for the transsphenoidal approach is dubious.

For pituitary tumor removal via transsphenoidal access, the da Vinci surgical system is commonly used [15]. It requires constant repositioning of the endoscope and visualization is also insufficient for proper tumor resection. A four-arm robotic system for skull base surgery through a single nostril is presented in [16]. A concentric tube-based dual-arm robotic system is also proposed [17] for the same surgical procedure. Both [16], [17] lack the ergonomic and anatomical design for the surgical procedure to be used in MRI. Thus, there is a need for a surgical system to comply with the anatomical and surgical constraints of the transsphenoidal procedure and can be deployed in an MRI environment.

Another limitation of the currently available tools and endoscopes (apart from the surgical procedure) is the proper stiffness for the procedure [18]. The stiffness should be minimum during navigation to the surgical site to avoid damage to the surrounding tissues. For procedures requiring tumor resection, high stiffness is preferred to hold the tool in its place and efficiently remove the tumor. Thus, the stiffness changing capability is vital for the surgical procedure to tune the stiffness according to the requirement. There are many stiffnesses changing solutions with different applications in the medical field [19]. A granular jamming-based approach is used in [20], [21] to vary the stiffness. A constraint tube-based approach is presented in [22] while a neutral line mechanism is proposed in [23] for stiffness variation in tendon actuated robots. A stiffness tunable catheter using the magnetic field is proposed for heart surgery [24]. An antagonistic actuation based shrinkable and inflatable manipulator is also another solution in literature [25]. A controller side stiffness variation of the active cannula is also done in [26]. A neurosurgical manipulator with shape memory alloy springs to vary stiffness by changing their state is also presented in [27]. It is deployable in the MRI, but the specific procedure in neurosurgery is not mentioned and it cannot be used through the transsphenoidal route due to high diameter ($>$10mm). All of these stiffness changing solutions [20]–[27] are mostly for the endoscopic surgery or lacks proper surgical application.

We propose a 6-degree-of-freedom (DOF) stiffness adjustable neurosurgical robot for pituitary tumor removal through the transsphenoidal route (shown in Fig. 1). The whole surgical system consists of two main parts; (1) robotic system with manipulator and actuation system that satisfy all the surgical and anatomical constraints and (2) MRI compatible motor system (ultrasonic motors and assemblies to transfer power to the robotic system). In this article, the design and working principle of the robotic system are mainly presented while the MRI compatible motor system [28] is under development and will be presented in the future.

The presented robotic system is designed to follow the anatomical and surgical constraints unlike [16], [17], [27]. It has a 6-DOF manipulator with 5mm and 1.5mm outer and inner diameters, respectively. The commercially available surgical tools can be used through the manipulator. A mechanical approach is used to vary the stiffness which can lift a force of more than 2N. A flexure shaft is designed, developed, and added to the manipulator to bend it at the required insertion angle to meet the surgical constraints. The manipulator is steered by a hybrid actuation system that is miniaturized, compact, and drives both CTR and TAR. The robotic system is designed according to the geometrical constraints of the Siemens®3-Tesla (3T) MRI bore. All the materials used for development are analyzed in MRI and the signal-to-noise ratios (SNR) are calculated.

The contributions of the presented work are: (1) a procedure and anatomy specific MRI compatible robotic system for pituitary tumor removal designed for a commercially available MR scanner, (2) design and optimization of the flexure shaft to satisfy the surgical requirement and (3) a task-specific stiffness changing solution to improve the surgical procedure.

Section II includes a clinical scenario, design of the robotic system, stiffness changing approach, the design and development of the manipulator, design, and optimization of flexure shaft and the actuation system. The stiffness changing capability is analyzed theoretically in section III. Section IV includes the experiments performed on the robotic system. The whole work is concluded in section V.

II. DESIGN & DEVELOPMENT

A. CLINICAL SCENARIO

The presented robotic system is designed for pituitary tumor resection under MRI. The patient is laid on the MRI bed and the robotic system is installed as shown in Fig. 1(a). The main steps of the surgical procedure are, (a) the manipulator is inserted in the nostril and move on to the sinus. (b) The sphenoid sinus is drilled to access the bony hollow, underside the brain. (c) Manipulator advances to the central skull base and reaches the pituitary gland. (d) The tumor is identified and resected using the surgical tools by teleoperation.

The ultrasonic motor module and the platform shown in Fig 1(a) are part of the MRI motor system [28], [29] which is under development and will be included in the future works.

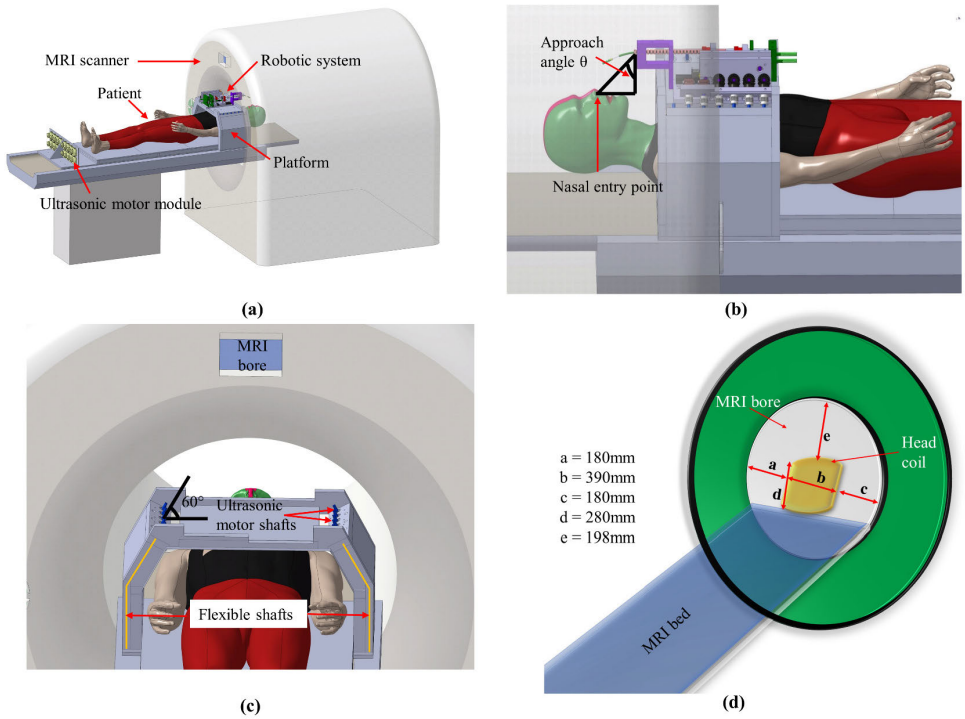

FIGURE 1. 3D model of the whole surgical system; (a) robotic system integrated with MRI compatible motor system and inserted in the bore of 3T MR scanner, (b) surgical constraint for insertion in the nasal cavity of the patient, (c) geometric constraints for the robotic system and (d) measured rough dimensions of the Siemens®3T MRI bore.

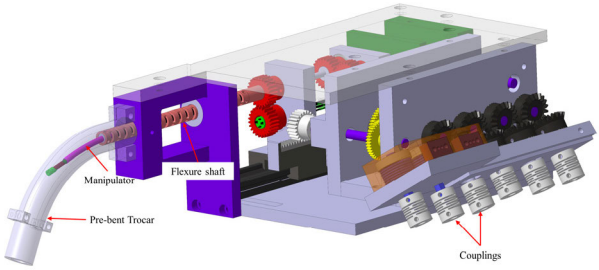

FIGURE 2. 3D model of the proposed 6-DOF robotic system.

TABLE 1. Constraints on the robotic system.

Constraints	Value
MR compatibility	SNR less than 30%
Geometric constraints of MRI bore	Ø478mm & Fig. 1(d)
Tilted angle of ultrasonic motor shafts	60°
Nasal cavity insertion angle	~70°
Stiffness changing capability	6 times or more
Insertion length	90mm [35]
Tip force	1.5N or more [38]

The 3D model of the robotic system presented here is shown in Fig. 2. As it is going to be used in MRI, all frame plates, gears, bolts, and shafts are of plastic. The only metal used is nitinol which is also MRI feasible and produces minimum artifacts [30]. The signal-to-noise ratio of the materials used in development is also calculated and presented in the experimentation section.

For insertion in the nostril of the patient, the manipulator should be bent at an angle θ demonstrated in Fig. 1(b). This θ is normally in the range of 70° [29] and depends on the anatomy, age, and gender of the patient but here it is taken as a constraint. Another constraint is the angle of ultrasonic motor shafts. These shafts are present on the platform at a 60° angle as shown in Fig. 1(c). The shaft angle is chosen according to the geometrical design of the MRI bore. The actuation system should be able to attach with those shafts for operation in the MRI room and provide a stroke of 90mm for insertion till the pituitary gland. Fig. 1(d) shows the measured dimensions of the 3T MR scanner with the head coil. The robotic system is designed according to these constraints and dimensions which are also presented in Table 1.

B. MANIPULATOR

1) DESIGN

A 6-DOF manipulator is designed for the surgical procedure by merging two different mechanisms: CTR and TAR. CTR are telescopic, pre-curved, and super elastic tubes actuated by their relative translation and rotation [31]. Tendon actuated robots are single or multi backbones controlled by pushing

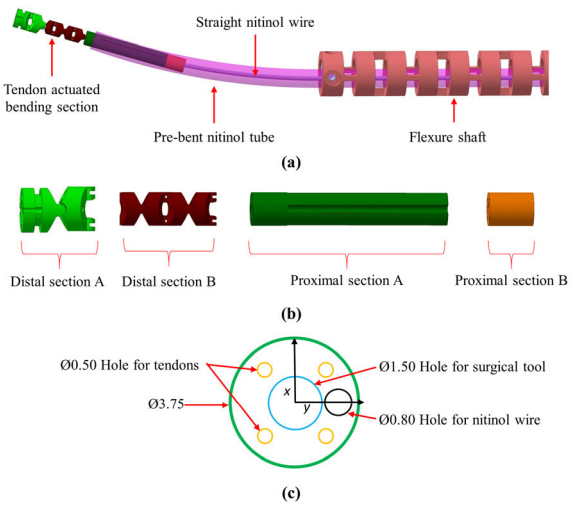

FIGURE 3. (a) 3D model of the 6-DOF manipulator, (b) elements of the tendon actuated bending section and (c) schematic design of the proximal section B.

and pulling of the tendons [32]. Both CTR and TAR are merged to benefit from there advantages and decrease their disadvantages. The 3D model of the designed manipulator is shown in Fig. 3(a). CTR is utilized to provide a higher stiffness in comparison to TAR which can assist in tumor resection, while it also covers a sufficient workspace at the surgical site [29]. TAR is used at the tip to provide higher maneuverability. A two-member CTR structure is used. It has one pre-bent outer tube and a straight inner nitinol wire while sliding joint based TAR are used on the distal side. The dimensions of the manipulator sections are provided in Table 2.

TABLE 2. Dimensions of the different manipulator sections.

Member	Outer diameter (mm)	Inner diameter (mm)	Length (mm)
Distal Section A	5.00	1.50	8.00
Distal Section B	3.75	1.50	16.00
Proximal Section A	3.75	1.50	3.00
Proximal Section B	3.75	1.50	5.00
Nitinol Tube	4.90	4.50	200 (total) 60 (pre-bent)
Nitinol Wire	1.18	-	280

The nitinol wire in the CTR arrangement is used to translate and rotate the tendon actuated bending section. It is a tricky part to use the wire and allow the hole for the surgical tool at the same time. To fulfill that purpose, a specially designed proximal section B (shown in Fig. 3(c)) is used. A total of six holes are fit in the Ø3.75mm section. Four of them are used for tendons while a Ø1.50mm central hole is made for the surgical tool. To incorporate the wire, a Ø0.80mm hole is made beside the surgical tool hole. To use the nitinol wire of Ø1.18mm (bigger than the Ø0.80mm hole), the end of the nitinol wire is grinded until it is reduced to Ø0.70mm at the tip which is inserted in the hole and glued. The nitinol wire of Ø0.80mm is quite flexible and deflect on small loads while Ø1.18mm nitinol wire has higher stiffness and efficiently transmit the forces applied at the base.

2) STIFFNESS CHANGING METHOD

To avoid damage to the sensitive brain tissues, the manipulator should have low stiffness but, for tumor removal, the stiffness should be higher. Therefore, a stiffness changing capability would likely improve the surgical procedure. Most of the stiffness changing solutions presented before cannot be installed in small diameter (Ø5mm) and they need an extra energy source (pneumatic, magnetic, or electric) which is difficult to be used in MRI. Therefore, a mechanical approach is used to change the stiffness of the manipulator. The idea is to change the stiffness with an approach that should not oppose the surgical and anatomical constraints and can be used in MRI. The designed manipulator has multiple parts of different materials and dimensions that can slide on each other. The exact theoretical model of such a manipulator is not available in the literature and it is beyond the scope of this work. But, if the manipulator is considered as a beam, then according to the beam theory, the deflection and stiffness are directly proportional to the length of the beam under the same boundary conditions. The manipulator is designed with weak (plastic resin) and strong (nitinol) parts that can slide over each other to vary the stiffness. If the length of the weaker part is increased, the stiffness decreases and vice versa considering the boundary conditions are the same.

In the designed manipulator, a total of six sliding joints are used at the distal section which are further divided into two sections as shown in Fig. 3(b). The distal section A has two sliding joints having Ø5.00mm which cannot be inserted inside the nitinol tube. The distal section B has four sliding joints with Ø3.75mm (smaller than the inner diameter (4.50mm) of the pre-bent nitinol tube) and they can easily be inserted in the nitinol tube decreasing the length of the weaker section (elastic modulus of tendon actuated part is 20 times lower than that of the nitinol tube). This mechanical approach is easily integrated into small dimensions of the manipulator. Furthermore, it can be controlled by the simple translation of the members and no external energy source of any kind is required. The maximum and minimum cases of stiffness are shown schematically in Fig. 4. The minimum stiffness is defined at the point where both distal section A and B are actuated while the maximum stiffness case is where only distal section A is outside the nitinol tube.

3) FLEXURE SHAFT

As stated before, the manipulator is required to bend at around 70° to be inserted through the nostril of the patient. To fulfill this surgical constraint, a flexure shaft is added to the manipulator. During the design procedure, the required bending

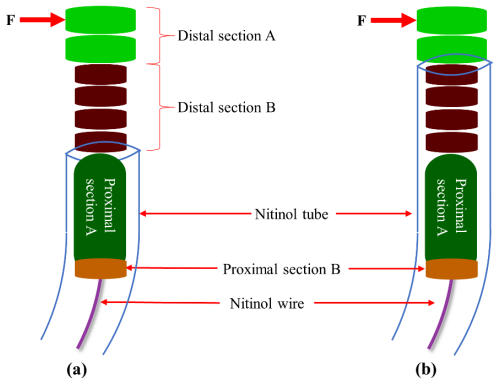

FIGURE 4. Stiffness changing approach; (a) minimum stiffness case and (b) maximum stiffness case.

angle (θ) for flexure shaft is set to be 80° for the safety margin. Elliptical hinge shape is chosen as it has minimum bending stiffness among conic section flexure hinges when geometric parameters are the same [33]. 3D model of the designed flexure shaft and the cross-sectional view of the hinges are shown in Fig. 5.

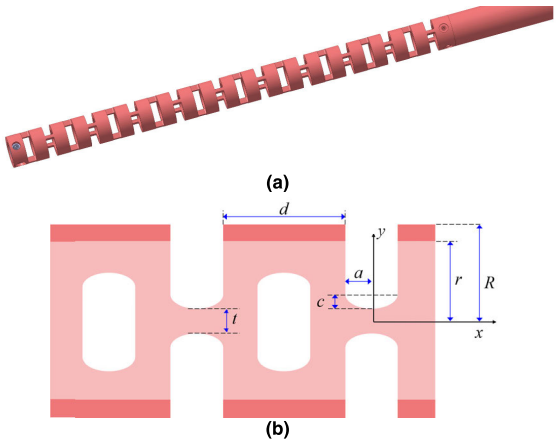

FIGURE 5. Designed flexure shaft (a) 3D model and (b) cross-sectional view of the elliptical hinges.

To design the flexure shaft, two main constraint equations are considered as follows:

$$4na + (2n-1)\,\mathrm{d} < l \tag{1}$$

$$n\tan^{-1}\frac{2a}{R} > \theta \tag{2}$$

Here, n is the number of hinges for one side (total number of the hinges is 2n), a is the axial radius and c is the lateral radius of elliptical conic section, d is the distance between two consecutive hinges, l is the total length of the bent part of the pre-bent trocar and R is the outer radius of the flexure shaft. Eq. (1) constraints for the total length of the flexure shaft that should be shorter than the length of the bent part of the pre-bent trocar and (2) defines the maximum allowable bending angle that should be larger than the required bending angle when the flexure hinge reaches the geometric limit. The rest of the parameters are solved according to these geometric constraints. Four parameters; a, c, n, and t are required to be solved for the geometry of the flexure shaft. Here, t is the flexure thickness. For the conic sections, a and c can be represented as two dimensionless constants β and γ [33].

$$\beta = \frac{t}{2c} \tag{3}$$

$$\gamma = \frac{t}{2a} \tag{4}$$

β, γ, n and t are the unknown parameters that are solved using the known parameters (d, R, r, and l). Here, d is 5mm, R is 6mm, r (inner radius of the flexure shaft) is 4mm and l is 160mm. PEEK is chosen as the material for flexure shaft and it has the elastic modulus E = 3.60 GPa and ultimate tensile stress $\sigma_u = 90$ MPa. The following cost function is defined to find parameters that minimize the maximum stress with respect to the stress concentration factor.

$$\text{Cost function} \;:\; f(\beta,\gamma)\times SF\times\frac{\theta}{n} \tag{5}$$

$$\frac{1}{f(\beta,\gamma)} = \frac{6}{Ebt^2}\frac{\beta}{(2+\beta)^2\gamma}\Big[\frac{3+4\beta+2\beta^2}{1+\beta} + \frac{6(1+\beta)}{\beta^{\frac{1}{2}}(2+\beta)^{\frac{1}{2}}}\tan^{-1}(1+\frac{2}{\beta})^{1/2}\Big]\ [33] \tag{6}$$

$$SF = \frac{\zeta+0.188}{\zeta+0.014}[34] \tag{7}$$

TABLE 3. Provided and optimized parameters of the flexure shaft.

Provided parameters	Value (mm)	Optimized parameters	Value (mm)
d	5	a	1.62
R	6	c	0.01
r	4	n	10
l	160	t_0	1.20

Here, $b = R-r$ while $\zeta = \frac{a^2}{c}$ and SF is the stress concentration factor. To solve the problem a factor of safety of 2 is applied. The hinge cross-section is assumed to be rectangular for analytical calculation of stress (the assumption is true if R is quite bigger than r). The defined cost function is optimized in MATLAB and the solved parameters are provided in Table 3. The maximum stress of the designed flexure shaft at 80° bending angle is 45.15 MPa with a factor of safety of 2. It is way below the ultimate strength and the geometrical limit of the flexure shaft with the optimized parameter was 284°, which, of course, means that the constraint (2) is satisfied. Therefore, the optimized parameters are rounded off and used for manufacturing.

Only one flexure shaft is used to bend the whole manipulator at 70° even though there are two CTR members: the outer tube and inner wire. The flexure shaft is attached to the outer nitinol tube as shown in Fig. 3(a) and the inner wire will bend with the flexure shaft and nitinol tube. If the inner CTR member is also a nitinol tube, another flexure shaft would be required for bending it at 70°. In the case of two flexure shafts, the issue of interference between the consecutive hinges is

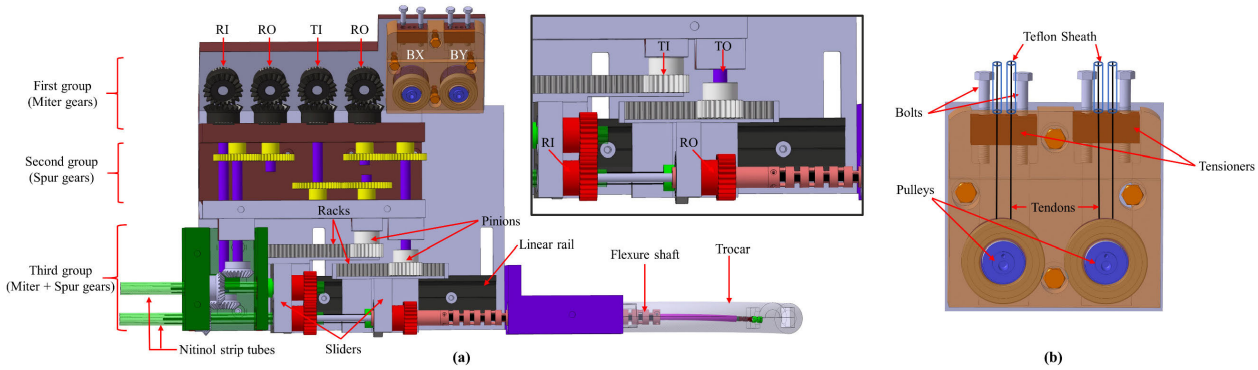

FIGURE 6. The designed actuation system (a) 3D model. Inset shows the rack and pinion combination for translation of concentric tube members. RI, RO, TI and TO represents the shafts responsible for rotation of inner and outer and translation of inner and outer CTR members, respectively while BX and BY represent the shafts for axial and lateral motion of tendon actuated section and (b) pulley and tensioner mechanism.

quite severe. Therefore, the nitinol wire is used as an inner member to avoid this issue.

C. ACTUATION SYSTEM

The platform attached to the MRI bed (as shown in Fig. 1(c)) has 60° oriented shafts due to the circular shape of the MRI bore. A 6-DOF hybrid actuation system is developed for CTR and TAR shown in Fig. 2 and Fig. 6 [35]. As the manipulator has 6-DOF, six ultrasonic motor shafts are required. For the actuation of CTR, three groups of gear assemblies are used on four shafts (RI, RO, TI, and TO) in the actuation system to transmit motor torque to the corresponding CTR members as shown in Fig. 6(a). The first group of gears is angled miter gears (bevel gears) to transmit the torques to shafts that are tilted at 60°. They allow the coupling of the actuation system to the shafts of the MRI compatible motor system as shown in Fig. 1(c). Spur gears are used in the second group to alter the distance and relative height between the input shafts. The third group is the gears that connect to the parts of the manipulator. For rotation, first miter and then spur gears are used. The miter gears rotate the shaft at 90° turning them in line to the CTR members. As the CTR members are concentrically placed and cannot be grasped at the base and rotated, the miter gear shafts rotate a nitinol strip-based plastic tube which in turn rotates the CTR members by the spur gears. In the case of translation, rack and pinion are used. Racks are attached to the sliders of the linear rail and the manipulator members are attached to these sliders while pinions are mounted on the shafts.

For the actuation of the bending section, the tendons need to be pushed and pulled. A pulley and tensioner mechanism are used for that purpose [29] as shown in Fig. 6(b). Nitinol wire of Ø0.22mm is used as tendons. The selection is made due to the MR compatibility and low hysteresis properties of nitinol wire. The nitinol tendons are covered in the Teflon sheath and passed on to two motor shafts (BX and BY). A pair of tensioners are used for four nitinol tendons. The Teflon sheath is glued to the tensioner while the inner tendons are passed down to the pulleys. Two tendons are wound on a single pulley and the rotation of the pulley in different directions will move the bending section in different axis. These pulleys are directly mounted on the motor shafts and supported by two plastic bearings to cancel out any lateral forces. The distance between the tensioner and pulley can be increased by the plastic bolts attached to the tensioner to adjust the tension and avoid sagging. The whole actuation system has dimensions of 240 × 175×112 mm (L×W×H). It is designed according to the geometrical constraints of the bore (Ø478mm) of the Siemens®3T MR scanner.

D. DEVELOPMENT

The prototype of the proposed robotic system is manufactured as in Fig. 7. As it is developed for MR guided surgical procedure, the choice of materials for development is limited to plastics and MRI compatible metals. The frame plates of the actuation system are manufactured with MC Nylon. Miter gears, linear rail, sliders, racks, and pinions are 3D printed using ABS, spur gears are of polyacetal, glass fiber reinforced PBT resin-based couplings and MC Nylon shafts are used. The flexure shaft is manufactured with PEEK. Nitinol tube and wires are used in the manipulator while the sliding joints are 3D printed using SLA. The bearings, nuts, and bolts are also of plastic resins. MR compatibility was tested, and SNR was also measured to verify the use of these materials (presented in section IV).

III. THEORETICAL ANALYSIS

A procedure-specific mechanical stiffness changing approach is introduced to assist the surgical process. The free-body diagram of the 6-DOF manipulator is shown in Fig. 8. The whole manipulator is divided into six sections having different materials with different cross-sectional areas. The first section (from 0 to L_1) has the flexure shaft holding the nitinol tube inside. The second section (L_1 to L_2) has the nitinol tube. The proximal section B and nitinol tube is the third section (L_2 to L_3). The fourth section consists of the proximal section A and nitinol tube from L_3 to L_4. Distal section B from L_4 to L_5 constitutes the fifth section. The stiffness can be changed by varying the length of this section as the distal section B can be inserted inside the nitinol tube.

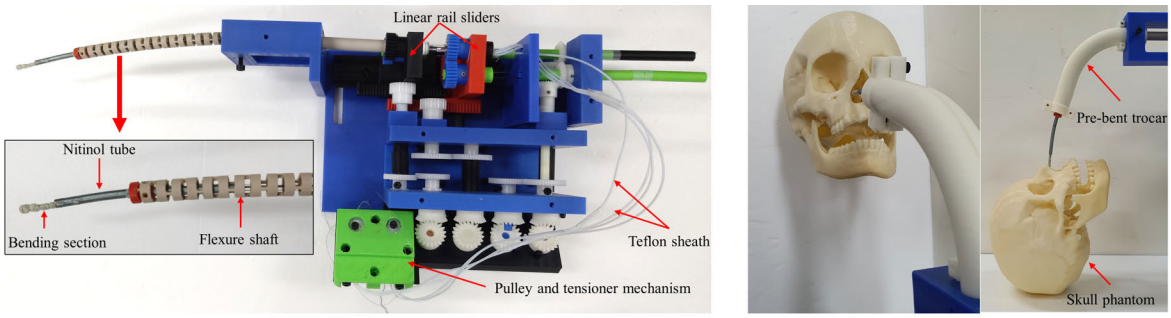

FIGURE 7. (a) The developed robotic system with inset showing 6-DOF manipulator and (b) the manipulator bent at 70° to access the nostril of skull phantom.

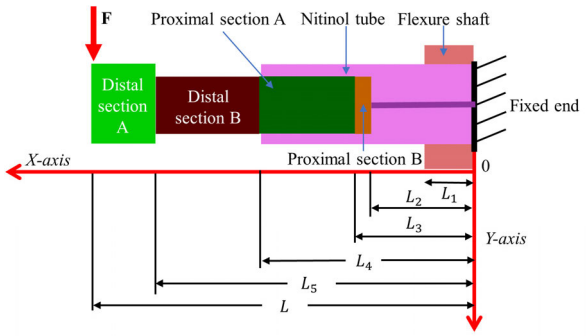

FIGURE 8. Free body diagram of the manipulator for theoretical analysis.

Sixth and the last section is the distal section A (L_5 to L) which cannot be inserted in the nitinol tube. A force **F** is applied on the tip of the manipulator and the proximal end of the flexure shaft is fixed. As the manipulator is quite complex having different sections, the exact model is not available in the literature. In this work, the theoretical model is derived using the Castigliano's theorem [36]. The strain energy stored in the manipulator due to bending is given by (8). As the manipulator is divided into six sections, the total strain energy is the function of the strain energy in each section. Therefore, (9) is formulated according to the designed manipulator having different materials and cross-sectional areas.

$$U = \int_0^L \frac{M^2}{2EI} dx \tag{8}$$

$$U = \begin{cases} \int_0^{L_1} \dfrac{(Fx)^2}{2(E_f I_f + E_n I_t)} dx, & 0 < x \leq \mathrm{L}_1 \\ \int_{L_1}^{L_2} \dfrac{(Fx)^2}{2E_n I_t} dx, & \mathrm{L}_1 < x \leq \mathrm{L}_2 \\ \int_{L_2}^{L_3} \dfrac{(Fx)^2}{2(E_s I_{psb} + E_n I_t)} dx, & \mathrm{L}_2 < x \leq \mathrm{L}_3 \\ \int_{L_3}^{L_4} \dfrac{(Fx)^2}{2(E_s I_{psa} + E_n I_t)} dx, & \mathrm{L}_3 < x \leq \mathrm{L}_4 \\ \int_{L_4}^{L_5} \dfrac{(Fx)^2}{2E_s I_{dsb}} dx, & \mathrm{L}_4 < x \leq \mathrm{L}_5 \\ \int_{L_5}^{L} \dfrac{(Fx)^2}{2E_s I_{dsa}} dx, & \mathrm{L}_5 < x \leq L \end{cases} \tag{9}$$

TABLE 4. Parameters used for theoretical analysis.

Parameter	Value
E_t	83 GPa
E_s	4.10 GPa
E_f	3.60 GPa
I_{psb}	$9.46\times 10^{-12}\mathrm{m}^4$
I_{psa}	$3.04\times 10^{-11}\mathrm{m}^4$
I_{dsb}	$9.46\times 10^{-12}\mathrm{m}^4$
I_{dsa}	$9.46\times 10^{-12}\mathrm{m}^4$
I_t	$8.17\times 10^{-12}\mathrm{m}^4$
I_f	$8.17\times 10^{-10}\mathrm{m}^4$

Here, F is the force applied on the tip, L is the total length of the beam, E is the elastic modulus and I is the second moment of the area. Also, E_f, E_n, and E_s are the elastic modulus of the flexure shaft, nitinol tube, and 3D printed sliding joints, respectively. As both proximal and distal sections are 3D printed using the same material, their elastic modulus is the same and denoted by E_s. I_f, I_t, I_{psb}, I_{psa}, I_{dsb}, and I_{dsa} are the second moment of area of the flexure shaft, nitinol tube, proximal section B, proximal section A, distal section A and distal section B, respectively. These parameters used for simulation are provided in Table 4. The strain energy calculated by (9) can be used to find the deflection δ of the manipulator under the applied load (10). The stiffness k of the manipulator can be calculated using (11).

$$\delta = \frac{2U}{F} \tag{10}$$

$$k = \frac{F}{\delta} \tag{11}$$

The stiffness of the proposed manipulator can be changed by varying the length of distal section B ($L_5 - L_4 = 16$mm (initial length)). For theoretical analysis and experimentation, the whole manipulator is categorized into three cases defined according to this length as shown in Fig. 9. Case 1 has minimum stiffness and case 3 has maximum while case 2 being the intermediate stiffness case. In other words, all the four sliding joints of distal section B are actuated in Case 1 and

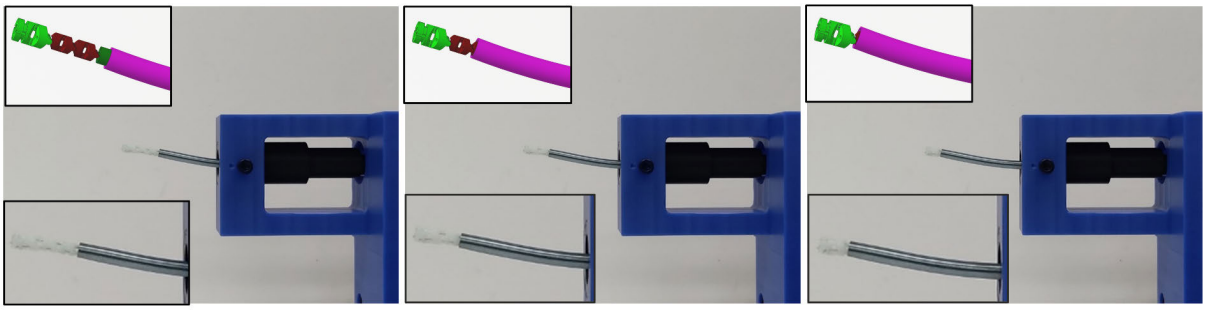

FIGURE 9. Three cases of different stiffness (a) Case 1 (minimum stiffness), (b) Case 2 (intermediate stiffness) and (c) Case 3 (maximum stiffness). Upper inset shows the 3D model of the manipulator configuration in each case and the bottom inset shows the same configuration in developed prototype.

TABLE 5. Theoretical and experimental stiffness for all the three cases.

Test #	δ (th) (mm)	F (th) (N)	δ (ex) (mm)	F (ex) (N)	k (th) (N/mm)	k (ex) (N/mm)
Case No. 1						
1.	2.38	0.48	5	0.48	0.20	0.09
2.	2.28	0.46	5	0.46	0.20	0.09
3.	2.18	0.44	5	0.44	0.20	0.09
4.	2.23	0.45	5	0.45	0.20	0.09
5.	2.33	0.47	5	0.47	0.20	0.09
Avg. k (N/mm)		0.09		RMS k (N/mm)		0.09
Case No. 2						
1.	2.34	0.96	5	0.96	0.41	0.19
2.	2.40	0.98	5	0.98	0.41	0.20
3.	2.37	0.97	5	0.97	0.41	0.19
4.	2.32	0.95	5	0.95	0.41	0.19
5.	2.32	0.95	5	0.95	0.41	0.19
Avg. k (N/mm)		0.19		RMS k (N/mm)		0.19
Case No. 3						
1.	3.81	4.66	5	4.66	1.22	0.93
2.	3.77	4.62	5	4.62	1.22	0.92
3.	3.74	4.58	5	4.58	1.22	0.92
4.	3.77	4.62	5	4.62	1.22	0.92
5.	3.75	4.59	5	4.59	1.22	0.92
Avg. k (N/mm)		0.92		RMS k (N/mm)		0.92

*Here, 'th' stands for theoretical simulation and 'ex' for experimental results. The average and RMS values are provided only for the experimental results.

$L_5 - L_4 = 16$mm. If two sliding joints of distal section B are actuated outside the nitinol tube, it is called Case 2 ($L_5 - L_4 = 8$mm). And if all the distal section B is inside the nitinol tube, it is Case 3 ($L_5 - L_4 = 0$mm). MATLAB®is used to solve (9) for the deflection of the manipulator on the known force values for all the three cases. These force values are from the experiments presented in section IV. The theoretical stiffness and deflection are presented in Table 5 and Fig. 12(b) in comparison with the experimental stiffness and deflection of the developed prototype.

IV. EXPERIMENTS & RESULTS

A series of experiments were performed to validate the characteristic of the proposed robotic system.

A. MR COMPATIBILITY TEST

The materials used in the development of the robot were tested for MR compatibility. 3T MR scanner *Skyra* from Siemens®was used for experimentation. Three combinations of materials were made, and MR images were obtained and analyzed to validate the compatibility and calculate the signal to noise ratio (SNR) as shown in Fig. 10. In the first combination (C1), the MR phantom containing $CuSo_4$ liquid was placed in the head coil and ten MR images were obtained. In C2, a 3D printed ABS tube, silicone tube and PEEK tube were placed in the head coil with the phantom. Lastly in C3, Reny plastic bolts of different sizes, nitinol wires and Teflon tubes of different diameters were placed in the head coil. The signal to noise ratio (SNR) in each combination was calculated using Nema4 method [37]. To calculate the signal value in the image, a region of interest (ROI) was chosen in the phantom image that includes 75% of the signal value. The mean pixel intensity in the ROI was the signal value. For noise, four rectangular ROIs were chosen at the corners of the image away from the signal and standard deviation in the pixel intensity for each ROI was calculated. These standard deviations were averaged and divided by 0.66 which is a Rician distribution correction factor to obtain the image noise [37]. Afterward, the signal value is divided by the calculated noise to get the SNR.

Since we had ten MR images for each combination, SNR in each image of every combination was calculated using MATLAB®and the mean and standard deviations were computed. As shown in Fig. 10, mean SNR in the $CuSO_4$ phantom image was 146.33% with a standard deviation of 5.44%. In C2 (ABS + PEEK + Silicon) and C3 (Reny bolts + Nitinol wire + Teflon tube) the calculated mean SNR was 136.81% ± 17.23 and 114.17% ± 6.90, respectively. As the SNR reduction was 6.50% in C2 and 9.70% in C3, the chosen materials for the robotic system are MR compatible.

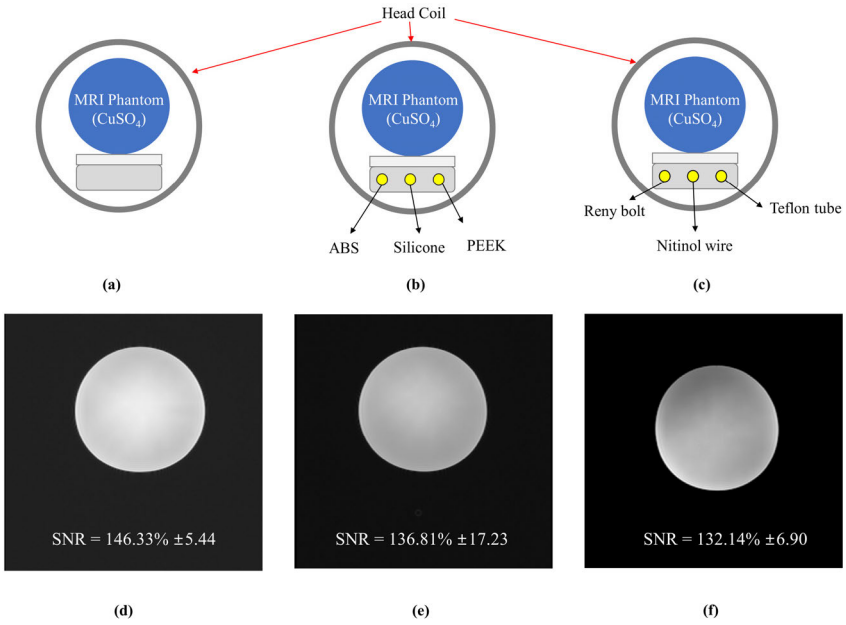

FIGURE 10. Signal-to-noise ratio calculation; (a, b, c) schematic setup for C1, C2 and C3 respectively, (d, e, f) MR image and SNR of C1, C2 and C3, respectively.

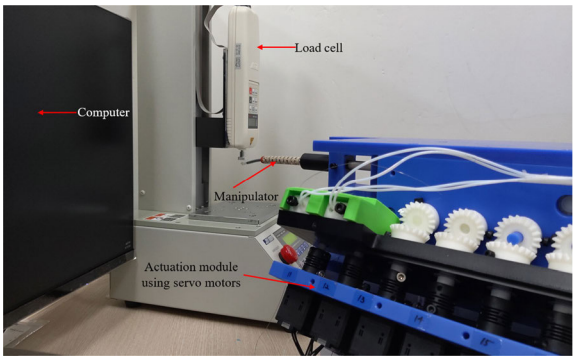

FIGURE 11. Setup for stiffness variation experiments.

B. STIFFNESS CHANGING CAPABILITY

To validate the theoretical analysis, stiffness changing experiments were performed using a universal load testing machine (JSV-H1000) from Japanese Instrumentation System Co. (JISC, Japan). It uses a load cell (HF-1) also from JISC, which provides values in gram force (gF) with a resolution of 0.01 gF. The experimental setup for experimentation is shown in Fig. 11. A deflection of 5mm was applied on the tip of the manipulator and the force required for that deflection was measured by the load cell. An actuation module using seven servo motors (Dynamixel) from ROBOTIS Inc., Korea was developed in the laboratory to drive the robotic system for experimentation purposes. First, the manipulator was actuated so that all the bending section B is outside the nitinol tube (as in Case 1), and the force required to produce a deflection of 5mm was measured. Then, the outer nitinol tube was actuated 8mm and the configuration of Case 2 was achieved. Lastly, the nitinol tube was actuated further 8mm and only two sliding joints of distal section A were outside becoming Case 3. Five experiments were carried out for each case and the results are provided in Table 5. The experiments were carried out with all the members held in their place. The tendons of the bending section were wound on the pulley and their tension was not changed during the experimentation.

In the experiments, deflection value was fixed to 5mm, and force was measured by the load cell in each case. For simulation, the amount of force measured during the experiment in each case was used, and the deflection was calculated. In this way, we have force and deflection data for both theoretical and experimental cases to calculate the stiffness using (11). Experimentally, the stiffness can be changed 10.22 times while theoretically it can be varied 6.10 times. The comparison of experimental and theoretical stiffness is shown in Fig. 12. The results validate that the proposed manipulator has stiffness changing capability for efficient tumor removal. The difference in the experimental and theoretical results is because the manipulator was modeled according to Castigliano's theorem excluding any non-linear factors. Also, the theoretical model is not exact due to the complexity of the manipulator having sliding parts with different dimensions and materials. Another major factor can be the assumption that for the theoretical analysis the gap between the flexure shaft and the trocar is zero, which is nonzero during experimentation. Still, the stiffness can be tuned more than the required value of 6 times, the proposed stiffness changing solution appears to be well suited for the surgical procedure.

C. MAXIMUM TIP FORCE

The manipulator should generate enough force to efficiently remove the tumor. The pituitary tumor resection force depends on the size and interaction with the type of tissues.

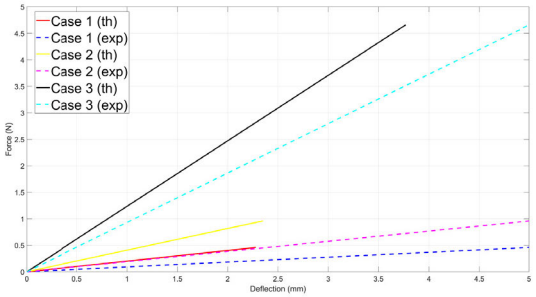

(a)

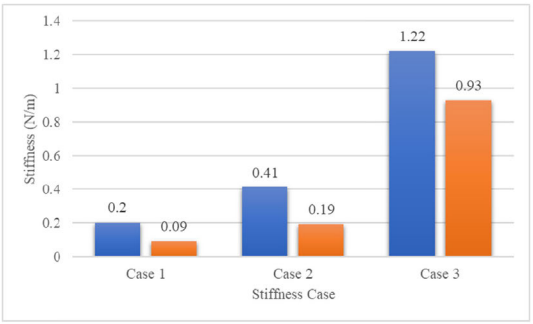

(b)

FIGURE 12. (a) Comparison of theoretical and experimental stiffness. Here 'th' stands for theoretical and 'exp' stands for experimentation and (b) theoretical and experimental stiffness for the three cases. Blue bars represent theoretical stiffness while orange ones represent the experimental stiffness.

TABLE 6. Results of the maximum tip force experimentation.

Experiment No.	Deflection (mm)	Force (N)
1.	2.50	2.20
2.	2.50	2.24
3.	2.50	2.26
4.	2.50	2.28
5.	2.50	2.28
6.	2.50	2.31
7.	2.50	2.25
8.	2.50	2.27
9.	2.50	2.26
10.	2.50	2.31
Mean		2.27
Standard deviation		0.03
Root mean square		2.27

For interaction with soft tissues, the average forces range from 0.1∼0.5N while with bony structures it can be as high as 2.12N [38]. 1.5N tip force was chosen as the design criterion for the proposed system and the maximum force generated at the tip of the manipulator was measured experimentally and the same universal load testing machine (JSV-H1000) was used. The load cell was moved downwards to 2.5mm and held there for 15 seconds. The manipulator tip was moved upwards by the actuation of distal section A to lift the load cell tip. As the target was to measure maximum tip force,

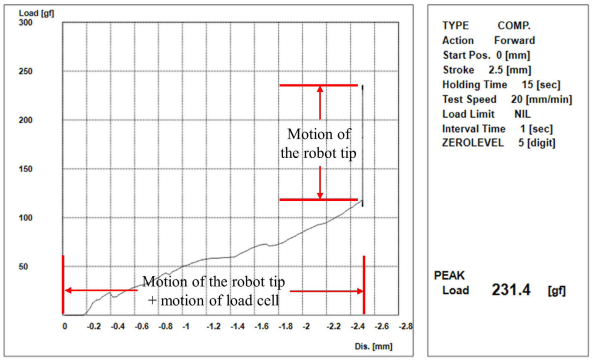

FIGURE 13. Force-deflection curve of mean tip force.

all the experiments were performed in the configuration of Case 3 (maximum stiffness). The experiments were repeated ten times and the results are provided in Table 6. Fig. 13 shows the force-deflection curve of the tip force measurement. The results show that the manipulator can lift a maximum force of 2.27±0.03N. Most of the pituitary tumors are less than Ø10mm [1] and the proposed manipulator can generate more force than the required value of 2.12N for bony and 0.1∼0.5N for soft tissue interactions. [38]. Another outcome of the maximum tip force experiment is that there was no case of failure during the 10 repeated trials. The presented prototype avoids failure even at maximum payload which makes it safe for the surgical task.

V. CONCLUSION AND FUTURE WORK

A stiffness adjustable 6-DOF robotic system is proposed in this work for pituitary tumor resection through the trans-sphenoidal approach. The system is designed specifically to operate in the bore of Siemens®3T MR scanner and it is the only system reported to date that follows the anatomical and surgical constraints of the trans-sphenoidal surgery with a stiffness changing capability. The proposed mechanical approach can vary stiffness ten times and is well suited for the surgical procedure and image acquisition platform. The manipulator can lift a force of more than 2N without failure. Experiments have also verified that the materials used for development are MRI compatible. The developed robotic system is miniaturized (240 × 175×112 mm, L×W×H) enough to fit inside the bore (Ø478mm) of the Siemens®3T MR scanner. The presented robotic system is the preliminary version and first part of the whole MR-guided surgical system. MRI compatible motor system (second part) is under development which will be integrated with the presented robotic system. Afterward, further experimentation and analysis will be performed.

For the future version, the kinematics of the 6-DOF manipulator will be solved and the final system will be a tele-operated one controlled outside of the MRI room. Also, the surgical tools are going to be integrated with the current robotic system. Secondly, the workspace subtended by the manipulator in all the three mentioned cases will be analyzed. The proposed stiffness changing solution is mechanical and

it is well suited for MRI conditions (no requirement of extra systems and electricity) but, it may affect the workspace. Third, the accuracy and repeatability of the robotic system after integration with the ultrasonic motor system will be tested. Lastly, the MR compatibility and SNR of the materials used for development are presented here but the MR-image may deteriorate during the motion of the robot. SNR of the whole robotic system in motion is beyond the scope of this work as the MRI-compatible motor system is under development and will be included in the future works. The results of the preliminary tests provided in this work endorse the need for further development and analysis.

REFERENCES

[1] V. Bagga and S. Sinha, "Surgery for pituitary tumours," *Surg. (Oxford)*, vol. 35, no. 10, pp. 556–562, Oct. 2017, doi: 10.1016/j.mpsur.2017.06.021.

[2] Y. Mohamadi, M. Mousavi, R. Pakzad, and G. Hassanzadeh, "Anthropometric parameters for access to sella turcica through the nostril," *J. Craniofacial Surg.*, vol. 27, no. 6, pp. e573–e575, Sep. 2016, doi: 10.1097/SCS.0000000000002879.

[3] F. A. Jolesz, "Invited. Interventional and intraoperative MRI: A general overview of the field," *J. Magn. Reson. Imag.*, vol. 8, no. 1, pp. 3–7, Jan. 1998, doi: 10.1002/jmri.1880080104.

[4] A. Albu, R.-E. Precup, and T.-A. Teban, "Results and challenges of artificial neural networks used for decision-making and control in medical applications," *Facta Universitatis, Ser., Mech. Eng.*, vol. 17, no. 3, p. 285, Nov. 2019, doi: 10.22190/FUME190327035A.

[5] Y. S. Kwoh, J. Hou, E. A. Jonckheere, and S. Hayati, "A robot with improved absolute positioning accuracy for CT guided stereotactic brain surgery," *IEEE Trans. Biomed. Eng.*, vol. 35, no. 2, pp. 153–160, Feb. 1988, doi: 10.1109/10.1354.

[6] H. Su, W. Shang, G. Cole, G. Li, K. Harrington, A. Camilo, J. Tokuda, C. M. Tempany, N. Hata, and G. S. Fischer, "Piezoelectrically actuated robotic system for MRI-guided prostate percutaneous therapy," *IEEE/ASME Trans. Mechatronics*, vol. 20, no. 4, pp. 1920–1932, Aug. 2015, doi: 10.1109/TMECH.2014.2359413.

[7] G. Srimathveeravalli, C. Kim, D. Petrisor, P. Ezell, J. Coleman, H. Hricak, S. B. Solomon, and D. Stoianovici, "MRI-safe robot for targeted transrectal prostate biopsy: Animal experiments: Transrectal prostate biopsy using a MRI-safe robot," *BJU Int.*, vol. 113, no. 6, pp. 977–985, Jun. 2014, doi: 10.1111/bju.12335.

[8] J. Tokuda, S.-E. Song, G. S. Fischer, I. I. Iordachita, R. Seifabadi, N. B. Cho, K. Tuncali, G. Fichtinger, C. M. Tempany, and N. Hata, "Preclinical evaluation of an MRI-compatible pneumatic robot for angulated needle placement in transperineal prostate interventions," *Int. J. Comput. Assist. Radiol. Surg.*, vol. 7, no. 6, pp. 949–957, Nov. 2012, doi: 10.1007/s11548-012-0750-1.

[9] V. Groenhuis, F. J. Siepel, J. Veltman, J. K. van Zandwijk, and S. Stramigioli, "Stormram 4: An MR safe robotic system for breast biopsy," *Ann. Biomed. Eng.*, vol. 46, no. 10, pp. 1686–1696, Oct. 2018, doi: 10.1007/s10439-018-2051-5.

[10] B. Yang, U.-X. Tan, A. B. Mcmillan, R. Gullapalli, and J. P. Desai, "Design and control of a 1-DOF MRI-compatible pneumatically actuated robot with long transmission lines," *IEEE/ASME Trans. Mechatronics*, vol. 16, no. 6, pp. 1040–1048, Dec. 2011, doi: 10.1109/TMECH.2010.2071393.

[11] G. R. Sutherland, I. Latour, and A. D. Greer, "Integrating an image-guided robot with intraoperative MRI," *IEEE Eng. Med. Biol. Mag.*, vol. 27, no. 3, pp. 59–65, May 2008, doi: 10.1109/EMB.2007.910272.

[12] M. Zimmermann, R. Krishnan, A. Raabe, and V. Seifert, "Robot-assisted navigated neuroendoscopy," *Neurosurgery*, vol. 51, no. 6, pp. 1446–1452, Dec. 2002, doi: 10.1227/01.neu.0000309121.39958.26.

[13] D. Hu, Y. Gong, B. Hannaford, and E. J. Seibel, "Semi-autonomous simulated brain tumor ablation with RAVENII surgical robot using behavior tree," in *Proc. IEEE Int. Conf. Robot. Autom. (ICRA)*, Seattle, WA, USA, May 2015, pp. 3868–3875, doi: 10.1109/ICRA.2015.7139738.

[14] G. Li, H. Su, G. A. Cole, W. Shang, K. Harrington, A. Camilo, J. G. Pilitsis, and G. S. Fischer, "Robotic system for MRI-guided stereotactic neurosurgery," *IEEE Trans. Biomed. Eng.*, vol. 62, no. 4, pp. 1077–1088, Apr. 2015, doi: 10.1109/TBME.2014.2367233.

[15] E. Y. Hanna, C. Holsinger, F. DeMonte, and M. Kupferman, "Robotic endoscopic surgery of the skull base: A novel surgical approach," *Arch. Otolaryngology–Head Neck Surg.*, vol. 133, no. 12, p. 1209, Dec. 2007, doi: 10.1001/archotol.133.12.1209.

[16] P. J. Swaney, J. M. Croom, J. Burgner, H. B. Gilbert, D. C. Rucker, R. J. Webster, III, K. D. Weaver, and P. T. Russell, III, "Design of a quadramanual robot for single-nostril skull base surgery," in *Renewable Energy Systems; Robotics; Robust Control; Single Track Vehicle Dynamics and Control; Stochastic Models, Control and Algorithms in Robotics; Structure Dynamics and Smart Structures*, vol. 3. Fort Lauderdale, FL, USA: ASME, Oct. 2012, pp. 387–393, doi: 10.1115/DSCC2012-MOVIC2012-8536.

[17] H. Gilbert, R. Webster, P. Russell, K. Weaver, and P. Swaney, "Endonasal skull base tumor removal using concentric tube continuum robots: A phantom study," *J. Neurological Surg. B, Skull Base*, vol. 76, no. 2, pp. 145–149, Nov. 2014, doi: 10.1055/s-0034-1390401.

[18] A. Loeve, P. Breedveld, and J. Dankelman, "Scopes too flexible...and too stiff," *IEEE Pulse*, vol. 1, no. 3, pp. 26–41, Nov. 2010, doi: 10.1109/MPUL.2010.939176.

[19] L. Blanc, A. Delchambre, and P. Lambert, "Flexible medical devices: Review of controllable stiffness solutions," *Actuators*, vol. 6, no. 3, p. 23, Jul. 2017, doi: 10.3390/act6030023.

[20] T. Ranzani, G. Gerboni, M. Cianchetti, and A. Menciassi, "A bioinspired soft manipulator for minimally invasive surgery," *Bioinspiration Biomimetics*, vol. 10, no. 3, May 2015, Art. no. 035008.

[21] A. Jiang, G. Xynogalas, P. Dasgupta, K. Althoefer, and T. Nanayakkara, "Design of a variable stiffness flexible manipulator with composite granular jamming and membrane coupling," in *Proc. IEEE/RSJ Int. Conf. Intell. Robots Syst.*, Oct. 2012, pp. 2922–2927.

[22] Z. Li, J. Feiling, H. Ren, and H. Yu, "A novel tele-operated flexible robot targeted for minimally invasive robotic surgery," *Engineering*, vol. 1, no. 1, pp. 073–078, Mar. 2015, doi: 10.15302/J-ENG-2015011.

[23] Y.-J. Kim, S. Cheng, S. Kim, and K. Iagnemma, "A stiffness-adjustable hyperredundant manipulator using a variable neutral-line mechanism for minimally invasive surgery," *IEEE Trans. Robot.*, vol. 30, no. 2, pp. 382–395, Apr. 2014, doi: 10.1109/TRO.2013.2287975.

[24] C. Chautems, A. Tonazzini, D. Floreano, and B. J. Nelson, "A variable stiffness catheter controlled with an external magnetic field," in *Proc. IEEE/RSJ Int. Conf. Intell. Robots Syst. (IROS)*, Sep. 2017, pp. 181–186, doi: 10.1109/IROS.2017.8202155.

[25] A. Stilli, H. A. Wurdemann, and K. Althoefer, "Shrinkable, stiffness-controllable soft manipulator based on a bio-inspired antagonistic actuation principle," in *Proc. IEEE/RSJ Int. Conf. Intell. Robots Syst.*, Sep. 2014, pp. 2476–2481.

[26] M. Mahvash and P. E. Dupont, "Stiffness control of surgical continuum manipulators," *IEEE Trans. Robot.*, vol. 27, no. 2, pp. 334–345, Apr. 2011, doi: 10.1109/TRO.2011.2105410.

[27] Y. Kim, S. S. Cheng, and J. P. Desai, "Active stiffness tuning of a spring-based continuum robot for MRI-guided neurosurgery," *IEEE Trans. Robot.*, vol. 34, no. 1, pp. 28–48, Feb. 2018, doi: 10.1109/TRO.2017.2750692.

[28] K. Cha, S. Seung, D. Kim, J. Lee, S. Jung, J. Choi, Y. Kim, C. Park, and S. Oh, "Driving apparatus of robot surgery system," (in Korean), Korean Patent 102 012 620, Aug. 20, 2019, doi: 10.8080/1020190026749.

[29] M. U. Farooq, K. Cha, D. K. Sohn, H. Yoo, and S. Y. Ko, "Design of a novel 6-DoF robotic system for pituitary tumor removal under MRI guidance," in *Proc. 19th Int. Conf. Control, Autom. Syst. (ICCAS)*, Jeju, South Korea, Oct. 2019, pp. 456–459, doi: 10.23919/ICCAS47443.2019.8971457.

[30] T. Duerig, A. Pelton, and D. Stöckel, "An overview of nitinol medical applications," *Mater. Sci. Eng., A*, vols. 273–275, pp. 149–160, Dec. 1999.

[31] P. E. Dupont, J. Lock, B. Itkowitz, and E. Butler, "Design and control of concentric-tube robots," *IEEE Trans. Robot.*, vol. 26, no. 2, pp. 209–225, Apr. 2010, doi: 10.1109/TRO.2009.2035740.

[32] J. Burgner-Kahrs, D. C. Rucker, and H. Choset, "Continuum robots for medical applications: A survey," *IEEE Trans. Robot.*, vol. 31, no. 6, pp. 1261–1280, Dec. 2015, doi: 10.1109/TRO.2015.2489500.

[33] N. Lobontiu, J. S. N. Paine, E. Garcia, and M. Goldfarb, "Design of symmetric conic-section flexure hinges based on closed-form compliance equations," *Mech. Mach. Theory*, vol. 37, no. 5, pp. 477–498, May 2002, doi: 10.1016/S0094-114X(02)00002-2.

[34] J. Wang and X. Liu, "Generalized equations for estimating stress concentration factors of various notch flexure hinges," *J. Mech. Design*, vol. 136, no. 3, Mar. 2014, Art. no. 031009, doi: 10.1115/1.4026265.

[35] M. U. Farooq and S. Young Ko, "A 6-DOF hybrid actuation system for a medical robot under MRI environment," in *Proc. 17th Int. Conf. Ubiquitous Robots (UR)*, Kyoto, Japan, Jun. 2020, pp. 165–168, doi: 10.1109/UR49135.2020.9144986.
[36] E. M. Odom and C. J. Egelhoff, "Teaching deflection of stepped shafts: Castigliano's theorem, dummy loads, heaviside step functions and numerical integration," in *Proc. Frontiers Educ. Conf. (FIE)*, Rapid City, SD, USA, Oct. 2011, pp. F3H-1–F3H-6, doi: 10.1109/FIE.2011.6143039.
[37] F. L. Goerner and G. D. Clarke, "Measuring signal-to-noise ratio in partially parallel imaging MRI," *Med. Phys.*, vol. 38, no. 9, pp. 5049–5057, Aug. 2011, doi: 10.1118/1.3618730.
[38] J. Bekeny, P. Swaney, P. Russell, K. Weaver, and R. Webster, "Forces applied at the skull base during transnasal endoscopic transsphenoidal pituitary tumor excision," *J. Neurological Surg. B, Skull Base*, vol. 74, no. 06, pp. 337–341, May 2013, doi: 10.1055/s-0033-1345108.

MUHAMMAD UMAR FAROOQ (Graduate Student Member, IEEE) received the B.S. degree in mechanical engineering from the Pakistan Institute of Engineering and Applied Sciences (PIEAS), Islamabad, in 2015, and the master's degree in mechanical engineering from Chonnam National University, South Korea, in 2017, where he is currently pursuing the Ph.D. degree. His research interests include surgical robots, medical instruments, and concentric tube robots.

HYUNWOO BAEK received the B.S. and M.S. degrees from the Korea Advanced Institute of Science and Technology (KAIST), Daejeon, South Korea, in 2016 and 2018, respectively, where he is currently pursuing the Ph.D. degree. His current research interest includes medical robots and control.

SUNGMIN SEUNG received the B.S. degree in mechanical engineering from Mokpo National University, Mokpo, South Korea, in 2008, and the M.S. and Ph.D. degrees from the Department of Mechanical Engineering, Chonnam National University, Gwangju, South Korea, in 2010 and 2015, respectively.

He is currently a Researcher with the Daegu-Gyeongbuk Medical Innovation Foundation (DGMIF), Daegu, South Korea. His research interests include medical robotics, surgical manipulator, and tele-operation control.

KYOUNGRAE CHA received the B.S., M.S., and Ph.D. degrees in mechanical engineering from Chosun University, Gwangju, South Korea, in 1996, 1999, and 2004, respectively.

From 2004 to 2008, he was a Research Associate with the Department of Mechanical Engineering and Aerospace, North Carolina State University, USA. From 2009 to 2012, he was the Principal Researcher Robot Research Initiative of Chonnam University, South Korea. From 2012 to 2020, he was a Principal Researcher with DGMIF, Daegu, South Korea. Since April 2020, he has been the Head of commercialization headquarter with the Korea Institute of Medical Microrobotics, Gwangju.

HEON YOU received the degree from the College of Medicine, Seoul National University, in 1989, and the Ph.D. degree in neurosurgery from the Graduate School of Medicine, Seoul National University, in 2001. He is currently the Chief Neurosurgeon of the National Cancer Center, South Korea. His main research interest includes brain tumors.

DONG-SOO KWON (Senior Member, IEEE) received the B.S. degree from Seoul National University, Seoul, South Korea, in 1980, the M.S. degree from the Korea Advanced Institute of Science and Technology (KAIST), Daejeon, South Korea, in 1982, and the Ph.D. degree from the Georgia Institute of Technology, Atlanta, in 1991, all in mechanical engineering. From 1991 to 1995, he was a Research Staff Member with the Oak Ridge National Laboratory. He is currently a Professor of mechanical engineering, the Director of the Center for Future Medical Robotics, and the Director of the Human–Robot Interaction Research Center, KAIST. His current research interests include human–robot interaction, medical robots, and haptics.

SEONG YOUNG KO (Member, IEEE) received the B.S., M.S., and Ph.D. degrees from the Department of Mechanical Engineering, Korea Advanced Institute of Science and Technology (KAIST), Daejeon, South Korea, in 2000, 2002, and 2008, respectively.

From 2009 to 2011, he was a Research Associate with the Mechatronics-In-Medicine Laboratory, Department of Mechanical Engineering, Imperial College London, U.K. He is currently a Professor with the School of Mechanical Engineering, Chonnam National University, Gwangju, South Korea. His research interests include medical robotics, human–robot interaction, and intelligent control.